Scripta Materialia 155 (2018) 144–148

Contents lists available at ScienceDirect

Scripta Materialia

journal homepage: www.elsevier.com/locate/scriptamat

Regular article

Elemental segregation to twin boundaries in a MnAl ferromagnetic Heusler alloy

D. Palanisamy *, D. Raabe *, B. Gault *

Max-Planck-Institut für Eisenforschung GmbH, 40237 Düsseldorf, Germany

ARTICLE INFO

Article history:
Received 15 May 2018
Received in revised form 16 June 2018
Accepted 18 June 2018
Available online xxxx

Keywords:
MnAl Heusler alloy
Massive transformation and twins
Solute segregation
Transmission electron microscopy (TEM)
Atom probe tomography (APT)

ABSTRACT

Electron microscopy and atom probe tomography were combined to investigate the crystallography and chemistry of a single twin boundary (TB) in a rare-earth-free ferromagnetic MnAl Heusler alloy. The results establish a significant segregation of Mn along the twin boundaries. An enrichment of approx. ~8 at.% Mn was measured along the twin boundary with a confined depletion outside the twin boundary, suggesting short range solute diffusion occurring during massive transformation.

The low-cost, binary Heusler $Mn_{55}Al_{45}$ intermetallic exhibits ferromagnetic properties [1] and is a promising rare-earth-free magnetic material that shows superior performance compared to ferrites [2–4]. The stoichiometric $Mn_{55}Al_{45}$ is an ordered compound that adopts a $L1_0$ structure (*P*4/*mmm* space group). This compound, identified as 'τ', is a metastable phase that evolves by suppressing the formation of equilibrium β-Mn (cubic) and γ_2 (Al_8Mn_5, rhombohedral) phases from the high temperature hexagonal-close packed (hcp) ε phase [1, 5]. The equilibrium phases are non-magnetic and their presence, even in trace fractions in the alloy, deteriorates the magnetic properties. The formation of these equilibrium phases can also be avoided either during controlled melt solidification [6–8] and/or by suppressing the τ phase decomposition [9, 10]. Recently, Mix et al. [10] reported that addition of Ga (5 to 9 at.%), replacing Al, makes the τ phase thermodynamically stable up to 700 °C with improved magnetic properties. Otherwise, τ decomposes into the β-Mn and γ_2 phases on prolonging heat treatment even at 450 °C.

Early reports of the ε-to-τ phase transformation indicated that the transformation is martensitic in nature [11, 12], while later investigations revealed a massive mode of transformation involving diffusional nucleation and growth phenomena [13–17]. In this mode, τ forms at grain boundaries within hcp-ε during cooling or isothermal annealing, and the moving interphase boundary of τ migrates, thereby consuming the ε grain with no specific crystallographic orientation relationship [18, 19]. During growth, the internal structure of τ develops lattice defects such as micro-twins, antiphase boundaries and dislocations [19, 20]. This is attributed to growth misplacements at the interphase boundary during its migration [19, 21, 22]. This defective structure is shown to influence the magnetic hysteresis of the ferromagnetic τ phase alloy [23, 24]. Recent investigations by micromagnetic simulations in this alloy reveal that twins act as domain wall nucleation and pinning sites and are thus responsible for reducing the external magnetic field required to nucleate these domain walls [25]. The alloy studied here has a high density of twins and is shown to have indeed a reduced maximum energy density product, $(BH)_{max}$, with ≈5% of the theoretical limit, 112 kJ/m^3, where B is the magnetic flux density and H is the magnetic field. Further processing such as extrusion and heat treatment can improve $(BH)_{max}$ through removing these defects from the microstructure [25].

Here, we present evidence that the twinning process involves a significant segregation of Mn along the twin boundaries. An approach combining transmission electron microscopy (TEM) and atom probe tomography (APT) [26] was used to reveal both crystallography and local composition of twins in a MnAl ferromagnetic Heusler alloy.

An ingot of nominal composition Mn - 45 at.% Al (constituent elements, 99.9% purity, Alfa Aesar) was synthesized by conventional vacuum arc-melting in high purity (99.999%) argon using a chilled water cooled copper hearth and a tungsten electrode. Initially, the mixed constituents are continuously heated at a slow rate up to the alloy's melting temperature followed by cooling for around 30 s under vacuum. This cycle was repeated at least three times and the overall composition progressively adjusted to compensate for the evaporation loss after each melting by addition of approx. 1.5 at.% Mn. This procedure was optimized such that no equilibrium nonmagnetic phases are formed. The ingot was subsequently heat treated at 1100 °C for 10 h in the single ε

* Corresponding authors.
E-mail addresses: d.palanisamy@mpie.de, (D. Palanisamy), d.raabe@mpie.de, (D. Raabe), b.gault@mpie.de (B. Gault).

https://doi.org/10.1016/j.scriptamat.2018.06.037
1359-6462/

phase regime followed by water quenching to retain ε at room temperature. The metastable τ is obtained by intermediate annealing at 450 °C for 5 h. To locate the twinned region and reveal the microstructure of the τ phase, a Zeiss Merlin scanning electron microscope (SEM, Carl Zeiss SMT, AG, Germany) equipped with a Gemini-type field emission gun electron column was used. The operating accelerated voltage of 30 kV with 4 nA probe current was applied. Additionally, the twinned region was confirmed by electron backscattered diffraction (EBSD) mapping that was carried out in JEOL-6500F field-emission SEM operated at 15 kV. The analysis of the EBSD data was carried out using the TSL OIM 6.2 software. The regions of interest were marked and site-specific atom probe specimens for correlative TEM and APT investigation were fabricated using a dual beam SEM/focused-ion-beam (FIB) instrument (FEI Helios Nanolab 600) with an in-situ lift-out procedure outlined in reference [27, 28]. The regions with the twinned structure were positioned and welded, by Pt deposition, on electropolished tips of a halved TEM Mo-grid mounted in a special correlative holder [29]. These were sharpened by FIB milling followed by a cleaning procedure at 5 kV and 8 pA current to remove damaged regions induced by Ga ion during high-energy (30 kV) milling. Diffraction studies by TEM on the APT tip was carried out using a Phillips CM-20 instrument operated at 200 kV. Atomic-scale compositional analysis was conducted by performing APT with the LEAP™ 5000XS instrument (Cameca Instruments). Laser pulsing mode was applied at a pulse repetition rate of 200 kHz and a pulse energy of 40 pJ. The specimen's base temperature was kept at 40 K and the target detection rate was set to be 5 ions detected every 1000 pulses. Data analysis was performed using the software package IVAS 3.8.0.

Fig. 1(a) shows an X-ray diffraction pattern for the sample annealed at 450 °C for 5 h. Diffractions peaks observed only pertain to the $L1_0$ ordered structure for the ferromagnetic τ phase with lattice parameters *a* and *b* as 2.77 Å and 3.54 Å respectively. No other diffraction peaks are present. Fig. 1(b) shows a backscattered electron (BSE) micrograph for the annealed sample. A high density of micro-twins is readily visible. EBSD mapping, as shown in Fig. 1(c), further confirmed the presence of these twins. The measured misorientation across the twin boundaries (A to B in inset Fig. 1(d)) is 75.6° as shown in the plot in Fig. 1(e). The misorientation angle corresponds to true twins and is consistent with the earlier report that these represent a major fraction of twins in MnAl alloy [23]. These micro-twins were of varying thickness ranging from ~10 nm to approx. 2 μm.

To confirm the origin of these twins, we present a BSE image in Fig. 2 (a) for the sample annealed at 450 °C for 15 min. It shows a ε phase grain boundary where τ nucleated as the starting stage of ε-to-τ phase transformation. The formation of micro-twins just behind the migrating interface boundary inside the massively transformed τ region is clearly revealed.

APT specimens were extracted at an inclined orientation as shown by the dashed red triangle in Fig. 2(a), to increase the probability for capturing at least one twin boundary. Fig. 2(b) shows a bright field (BF) image of an APT specimen in which twins appear with a dark contrast across the entire specimen. Fig. 2(c) shows the selected area diffraction (SAD) pattern from the region indicated by the white circle in Fig. 2(b). The diffraction pattern could be indexed as [101] zone axis corresponding to the τ phase. In addition to the matrix spots, we also

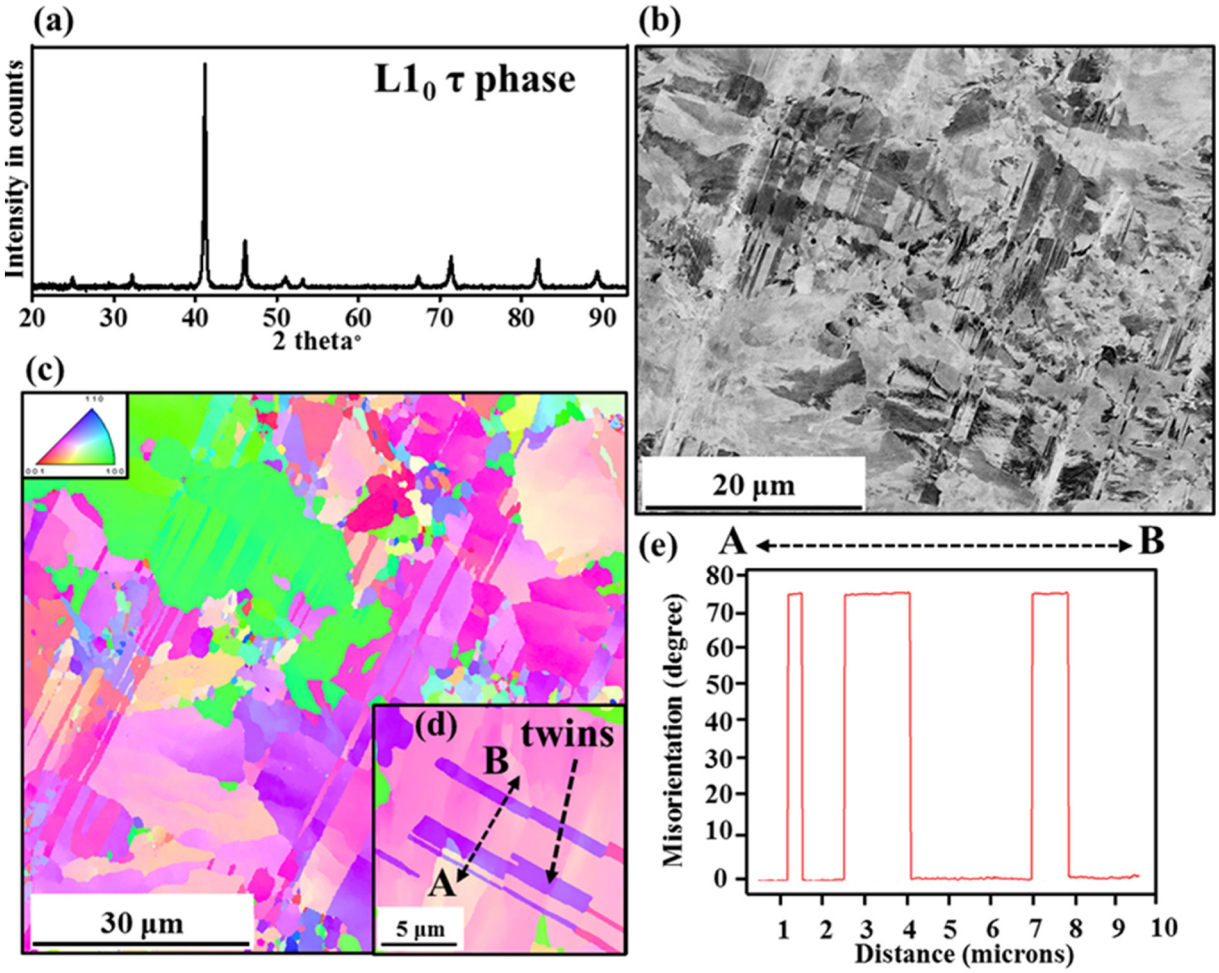

Fig. 1. (a) X-ray diffraction evidence for complete τ phase in the sample annealed at 450 °C for 5 h. (b) Backscattered electron (BSE) image for τ phase microstructure showing the presence of high density of micro-twins. (c) Electron backscattered diffraction (EBSD) map of a τ phase area showing evidence of micro-twins in the microstructure. (d) EBSD map for few micro-twins and (e) the misorientation plot across the twin boundaries (along AB).

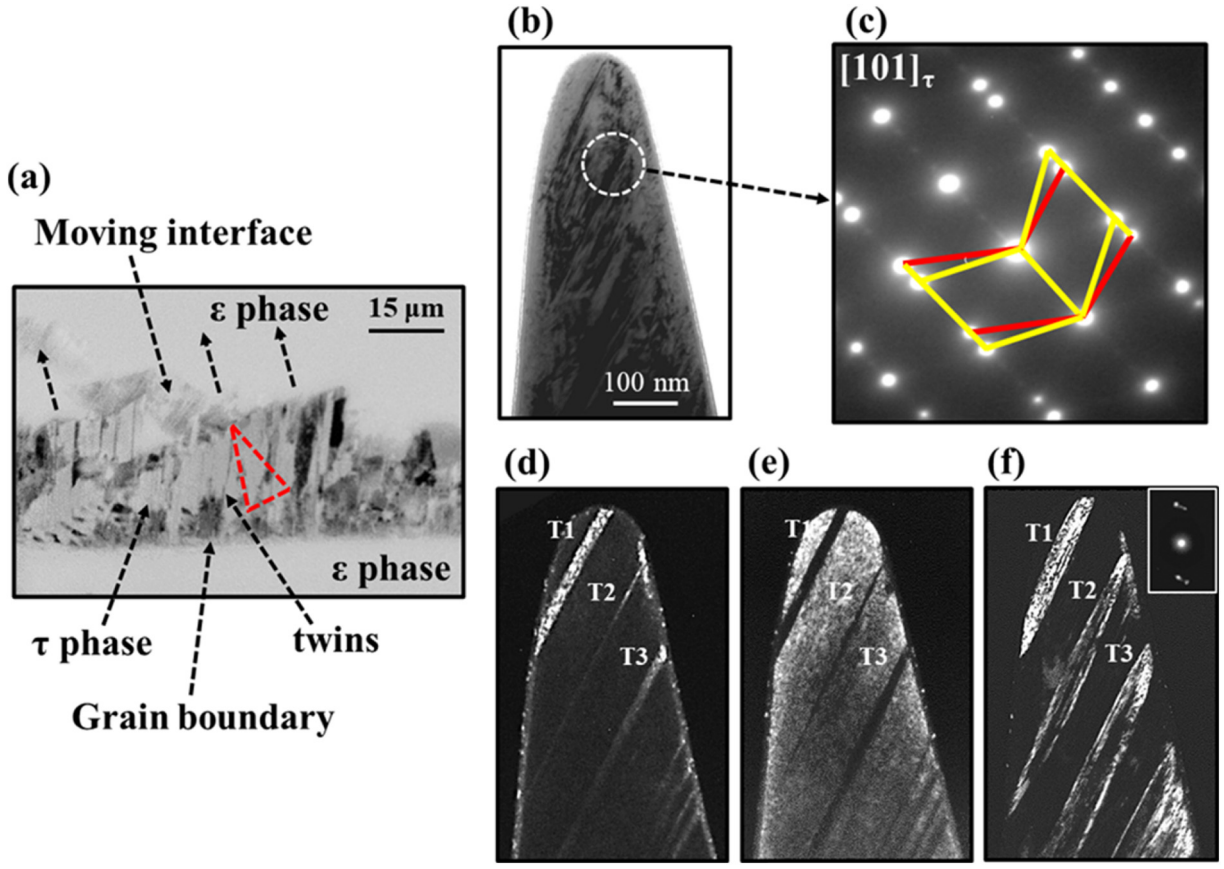

Fig. 2. (a) BSE image for the ε phase sample annealed at 450 °C for 15 min showing massive growth of τ phase on ε phase grain boundaries. The red triangle is the location from where the atom probe tips have been extracted. (b) Bright field (BF) image of the APT tips taken near to two beam [101] τ phase zone axis (c) Diffraction pattern taken from the circled location (white) on the tip indexed in terms of [101] τ phase zone axis with the additional twinning spots (d) Darkfield (DF) image taken from the twinning spot (e) DF image taken from nearby matrix spot (f) DF image taken form twinning spot in two-beam condition. (For interpretation of the references to color in this figure legend, the reader is referred to the web version of this article.)

observe extra twinning spots. With the orientation of the diffraction pattern and the BF image, the twin boundary can be indexed as $(\bar{1}11)$. Further, Fig. 2(d) and (e) show the comparison of dark field (DF) images taken from nearby matrix and twinning spots. The DF images clearly show the reflection of three twins present in the APT specimen marked as T1, T2, and T3. T1 and T3 have a similar thickness of approx. 50 nm while T2 is finer, only approx. 6 nm. These images were taken near to the [101] zone, i.e. at an edge-on perspective to the twin. Fig. 2(f) also shows the DF images taken from the twinning spot near to the two-beam tilting condition. Reflections from the complete twinned region with its boundary passing across the tip are clearly visible.

After TEM analysis, APT was performed on this specimen. Fig. 3(a) displays the APT reconstruction showing the distribution of Al in green. An iso-composition surface (red) contours regions in the APT reconstruction containing over 60 at.% Mn, and reveals solute enrichment confined along planar features. Their inclination matches the twin boundary planes visible in the DF image in Fig. 2(d). Fig. 3(b) shows a 2D composition map for Mn within the entire tip projected on the plane perpendicular to the viewing direction. The Mn solute fluctuations are clearly correlated to each of the twins T1, T2 and T3. Fig. 3 (c) shows 110 atomic planes across the T2 twin boundary. The planes become discontinuous at the twinning boundary showing the change in relative orientation at the boundary and enrichment of Mn atoms. The detector ion maps above and below T2, as shown in Fig. 3(d), are in the same orientation.

Fig. 4(a) shows the magnified 2D composition plot view corresponding to the dashed black rectangle superimposed to T2 in Fig. 3(b). The corresponding one-dimensional composition plot across this twin also shown. The Mn segregates to a maximum value of approx. 61 at.% while the Al depletes to a minimum value of 39 at.% exactly at the center of the twin. Otherwise, the Mn segregation is present throughout up to approx. ~5 nm thickness. The regions, approx. ~2.5 nm, on both sides of the twin, show Mn solute depletion down 2.5 at.% compared to the untwined region composition. To determine whether this solute segregation is occurring across the twinned region or if it is confined only to the twin boundaries, similar 2D composition plot were obtained for the thicker T1 twin from the region shown in Fig. 4(b). Interestingly, the Mn enrichment was found to be confined only to the actual twin boundaries and not to the twin interiors. The composition profile across the twin thickness shows similar Mn enrichment, however, a difference in values by ~1.5 at.%Mn is observed between the two boundaries enclosing the twin. Another difference is that the Mn enrichment was observed only across a ~2.5 nm thick region at both boundaries. Like for the thin twin, a confined Mn depleted region also was observed outside the twin boundaries but with different composition values. Detailed analysis of the 2D composition plot reveals that the Mn segregation along the boundary plane is varying.

This work shows first evidence of solute segregation, here Mn in $Mn_{55}Al_{45}$, along the twin boundaries formed during massive transformation. The twins observed herein are close to typical annealing twins ($\sum 3$ boundaries), which are low energy coherent boundaries. Due to their low interfacial energy, solute segregation to these boundaries is expected to be low compared to high angle grain boundaries (HAGB) [30]. However, in twinning induced plasticity (TWIP) steels [31], trace solute segregation of B, Si and P were measured to $\sum 3$ annealing twin boundaries along with a significantly higher segregation to a typical HAGB. Similar phenomena were observed in various other systems such as in deformed and annealed Mg-Zn-Gd [32], deformed Mg-Zn-Y

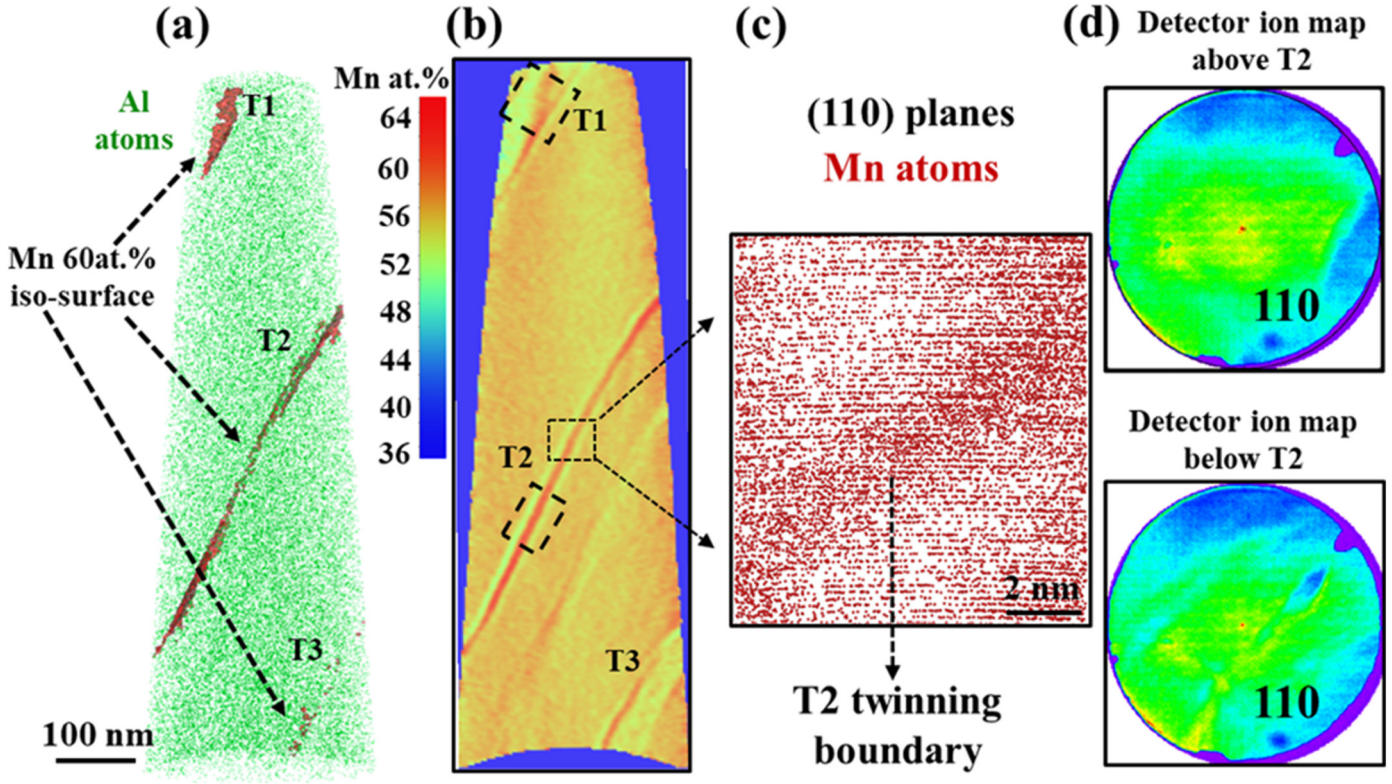

Fig. 3. (a) Atom probe reconstruction showing distribution of Al atoms (green color) and iso-composition interfaces with 60 at.% Mn (red color) showing Mn enrichment confined to T1, T2 and T3 twins. (b) 2D composition plot with scale for Mn across the APT tip reconstruction projected to the plane perpendicular to the viewing direction. (c) (110) Atomic planes across the T2 twin boundary. (d) Detector ion maps above and below the twinning boundary T2 showing same orientation. (For interpretation of the references to color in this figure legend, the reader is referred to the web version of this article.)

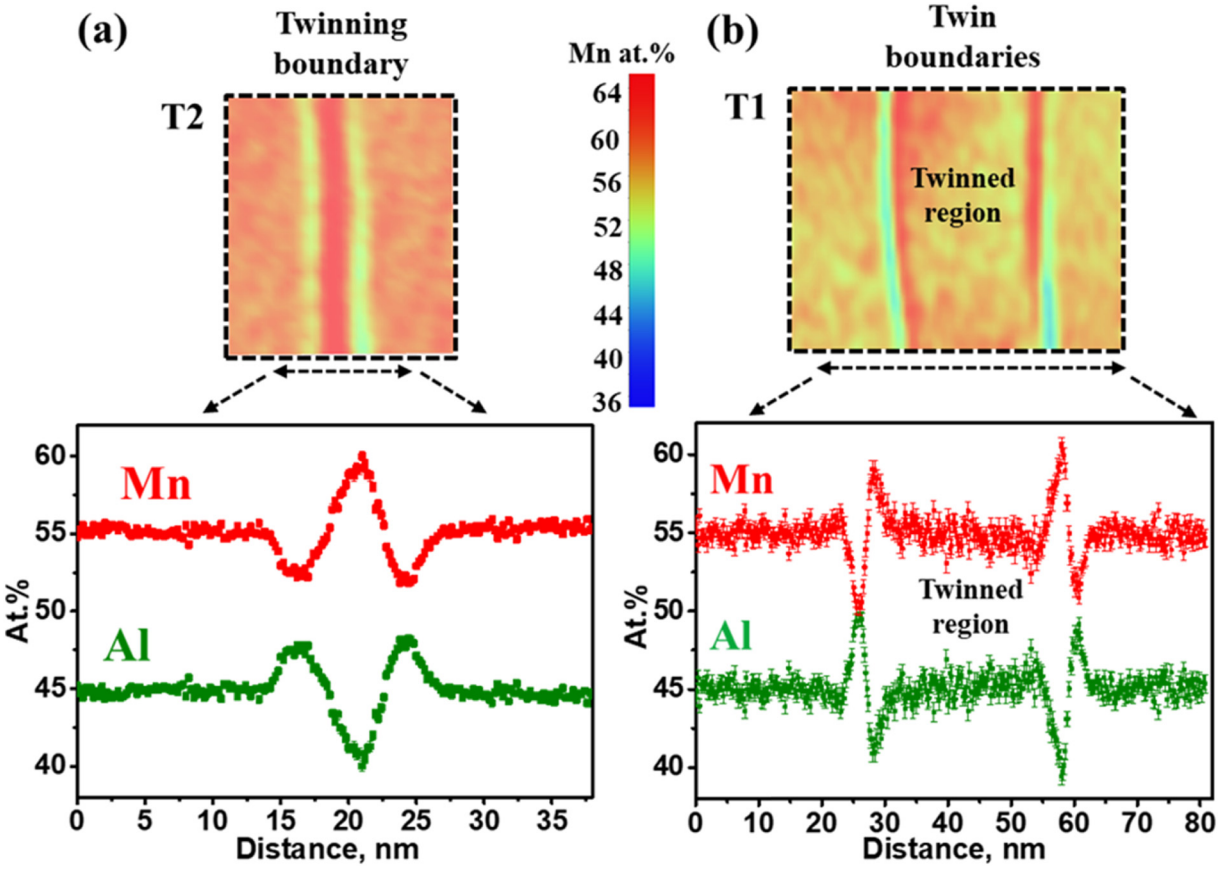

Fig. 4. (a) 2D and 1D composition plots across the twins (a) T2 and (b) T1 showing Mn enrichment confined to only the twin boundaries.

[33, 34], as well as in Ni- and Co-based superalloys, where Cr and Co segregations have been observed during creep deformation [35, 36]. These were attributed to long-range solute diffusion to the advancing partial dislocations that are responsible for the formation of these micro-twins.

The present case is different from these reports. We propose that the segregation we observe is related to a short-range solute diffusion phenomenon taking place simultaneously with the structural phase transformation with the migration of the interphase boundary from τ into the ε grain during heat treatment at 450 °C, 15 min. Yanar et al. [19] showed by high-resolution electron microscopy the formation of micro-twins in MnAl $L1_0$ ordered structure following the model proposed by Mahajan [22] on the annealing twin formation in fcc structures. In this model, the origin of micro-twins is related to the atomic attachment faults due to formation Shockley partial loops on {111} micro-facets of the migrating incoherent τ phase boundary. In addition to micro-twins, arrays of Shockley partials and antiphase boundaries (APBs) have been also observed in the massively transformed τ phase. However, until now, the local, near-atomic scale compositional fluctuations at these nanoscale defects were largely unknown.

The accurate compositional gradients across the twins obtained in the present work reveal several effects: First, short-range diffusion of Mn atoms to twin boundaries is occurring during massive phase transformation of ε to τ phase in this alloy. The Mn depletion zone near the twin boundary shows diffusion occurring from this depleted zone into the twin boundary plane. Second, in thicker twins, the variation of Mn segregation confined along the twin boundaries shows evidence of dynamic solute transport occurring along the twin boundary plane during heat treatment (450 °C, 15 min for the present case). These solute segregation and diffusional effects are expected to have direct implications on the nucleation of the equilibrium β-Mn and γ_2 (Al_8Mn_5-rhombohedral) phase and thus likely contribute to the decomposition of the metastable τ phase. However, these effects have to be further experimentally demonstrated, which will form the basis of future work, aiming to link these segregations to local measurements of the magnetic properties of the alloy.

Acknowledgments

The authors are grateful to U. Tezins and A. Sturm for their technical support of the atom probe tomography and focused ion beam facilities at the Max-Planck-Institut für Eisenforschung.

References

[1] H. Kōno, J. Phys. Soc. Jpn. 13 (1958) 1444.
[2] J.M.D. Coey, Scr. Mater. 67 (2012) 524.
[3] L.H. Lewis, F. Jiménez-Villacorta, Metall. Mater. Trans. A 44 (2013) 2.
[4] M.J. Kramer, R.W. McCallum, I.A. Anderson, S. Constantinides, JOM 64 (2012) 752.
[5] D. Palanisamy, C. Srivastava, G. Madras, K. Chattopadhyay, J. Mater. Sci. 52 (2017) 4109.
[6] A.E. Berkowitz, J.D. Livingston, J.L. Walter, J. Appl. Phys. 55 (1984) 2106.
[7] Y.J. Kim, J.H. Perepezko, J. Appl. Phys. 71 (1992) 676.
[8] D. Palanisamy, S. Singh, C. Srivastava, G. Madras, K. Chattopadhyay, Metall. Mater. Trans. A 1 (2016).
[9] T. Ohtani, N. Kato, S. Kojima, K. Kojima, Y. Sakamoto, I. Konno, M. Tsukahara, T. Kubo, IEEE Trans. Magn. 13 (1977) 1328.
[10] T. Mix, F. Bittner, K.-H. Müller, L. Schultz, T.G. Woodcock, Acta Mater. 128 (2017) 160.
[11] J.J. Van Den Broek, H. Donkersloot, G. Van Tendeloo, J. Van Landuyt, Acta Metall. 27 (1979) 1497.
[12] S. Kojima, T. Ohtani, N. Kato, K. Kojima, Y. Sakamoto, I. Konno, M. Tsukahara, T. Kubo, AIP Conf. Proc. 24 (1975) 768.
[13] A.V. Dobromyslov, A.E. Ermakov, N.T. Taluts, M.A. Uimin, Phys. Status Solidi A 88 (1985) 443.
[14] D.P. Hoydick, E.J. Palmiere, W.A. Soffa, J. Appl. Phys. 81 (1997) 5624.
[15] D.P. Hoydick, E.J. Palmiere, W.A. Soffa, Scr. Mater. 36 (1997) 151.
[16] C. Yanar, J.M.K. Wiezorek, W.A. Soffa, V. Radmilovic, Metall. Mater. Trans. A 33 (n.d.) 2413.
[17] Y.J. Kim, J.H. Perepezko, Mater. Sci. Eng. A 163 (1993) 127.
[18] H.I. Aaronson, Metall. Mater. Trans. A 33 (2002) 2285.
[19] C. Yanar, V. Radmilovic, W.A. Soffa, J.M.K. Wiezorek, Intermetallics 9 (2001) 949.
[20] H.I. Aaronson, S. Mahajan, G.R. Purdy, M.G. Hall, Metall. Mater. Trans. A 33 (2002) 2347.
[21] S. Mahajan, C.S. Pande, M.A. Imam, B.B. Rath, Acta Mater. 45 (1997) 2633–2638.
[22] S. Mahajan, Scr. Mater. 68 (2013) 95.
[23] F. Bittner, L. Schultz, T.G. Woodcock, Acta Mater. 101 (2015) 48.
[24] F. Bittner, J. Freudenberger, L. Schultz, T.G. Woodcock, J. Alloys Compd. 704 (2017) 528.
[25] S. Bance, F. Bittner, T.G. Woodcock, L. Schultz, T. Schrefl, Acta Mater. 131 (2017) 48.
[26] M. Herbig, Scr. Mater. 148 (2018) 98.
[27] P.J. Felfer, T. Alam, S.P. Ringer, J.M. Cairney, Microsc. Res. Tech. 75 (2012) 484.
[28] S.K. Makineni, M. Lenz, P. Kontis, Z. Li, A. Kumar, P.J. Felfer, S. Neumeier, M. Herbig, E. Spiecker, D. Raabe, B. Gault, JOM (2018) 1.
[29] M. Herbig, P. Choi, D. Raabe, Ultramicroscopy 153 (2015) 32.
[30] M. Herbig, D. Raabe, Y.J. Li, P. Choi, S. Zaefferer, S. Goto, Phys. Rev. Lett. 112 (2014), 126103. .
[31] M. Herbig, M. Kuzmina, C. Haase, R.K.W. Marceau, I. Gutierrez-Urrutia, D. Haley, D.A. Molodov, P. Choi, D. Raabe, Acta Mater. 83 (2015) 37.
[32] J.F. Nie, Y.M. Zhu, J.Z. Liu, X.Y. Fang, Science 340 (2013) 957.
[33] D.A. Basha, R. Sahara, H. Somekawa, J.M. Rosalie, A. Singh, K. Tsuchiya, Scr. Mater. 124 (2016) 169.
[34] D. Guan, J. Nutter, J. Sharp, J. Gao, W. Mark Rainforth, Scr. Mater. 138 (2017) 39.
[35] D. Barba, S. Pedrazzini, A. Vilalta-Clemente, A.J. Wilkinson, M.P. Moody, P.A.J. Bagot, A. Jérusalem, R.C. Reed, Scr. Mater. 127 (2017) 37.
[36] L.P. Freund, O.M. Messé, J.S. Barnard, M. Göken, S. Neumeier, C.M. Rae, Acta Mater. 123 (2017) 295.